One-Pot Synthesis of SnO₂/CNT Composite Anode Combined with Nickel Foam as a Current Collector for Lithium Ion Batteries

GUOQING ZHANG[1], CHENGZHAO YANG[1,*], LEI ZHANG[1] and LI MA[2]

[1]Faculty of Materials and Energy, Guangdong University of Technology, Guangzhou, P.R. China
[2]McNair Technology Co. Ltd., Dongguan 523800, P.R. China

*Corresponding author: E-mail: aixiny10@yahoo.com.cn

SnO₂/carbon nanotube (CNT) composites were prepared by a simple liquid-phase precipitation and subsequent heat treatment at 350 ºC. The samples were characterized by scanning electron microscopy, X-ray diffraction. The electrochemical measurements indicate that the high SnO₂ content composite using nickel foam as a conductive collector displays the best electrochemical performance with the specific capacity of 481 mAh g⁻¹ after 30 cycles at a current density of 200 mA g⁻¹ as anode for lithium ion batteries. This can be ascribed to the cushion effect of carbon nanotube and connection enhancement between the active material and conductive collector.

Key Words: Tin oxide, Carbon nanotube, Composite, Nickel foam, Lithium ion batteries.

INTRODUCTION

Currently, Li-ion batteries have become desirable energy storage devices for applications ranging from portable electronic devices to electric/hybrid vehicles[1]. Tin dioxide has been investigated extensively as one of the most promising substitutes for the graphite anode in Li-ion batteries because it has theoretical specific capacity (782 mAh g⁻¹) as twice as graphite[2]. However, large volume change during the intercalation and de-intercalation processes has a profoundly negative influence on the capacity retention[3]. The intrinsically induced drastic volume expansion causes a so-called pulverization problem which blocks the electrical contact pathways between adjacent particles, ultimately leading to rapid capacity fading[4].

Two strategies have been exploited in order to increase the cycling stability of tin-based oxide electrodes. One is to synthesize nano-tin dioxide with specific structures, such as core/shell structures[5], hollow structures[6,7], nanosheet[8] and nanorod[9]. However, the complicated procedures and high cost for synthesizing the nanostructured materials are still the main hindrance to the commercial use of SnO₂. The other is to disperse SnO₂ into a "buffering" carbon matrix that could alleviate the mechanical effects of the volume changes and the latter method is preferable due to the low cost and relatively simple process. Tin dioxide coated with buffering material exhibited better electrochemical performance than the bare material[10-12]. At present, SnO₂/carbon nanotube (CNT) composite have attracted considerable research efforts[13-15]. This is because CNTs can not only buffer the volume expansion, but also form an electric network and have high conductivity and large surface area[16].

Here, we found that SnO₂/CNT supported on the nickel foam exhibits good capacity and rate capability. SnO₂/CNTs composites were prepared by a liquid-phase precipitation. Substrate nickel foam, which has been widely applied in Ni-H battery, can provide large surface area per unit volume as a current collector. Moreover, the spongy-like current collector can facilitate the percolation of the electrolyte, thus provide an enhanced electrolyte accessibility and ion transferability[17,18]. The purpose of the study was to develop a simple method of preparing a SnO₂/CNTs composite for use as a lithium-ion battery anode with improved cycling stability by applying cheap and widely available process.

EXPERIMENTAL

The multi-walled carbon nanotubes (95 %, 20-40 nm) used in this work were purchased from Shenzhen Nanotech Port Co. Ltd. (Shenzhen, China) without any pre-treatment. The CNTs and H₂C₂O₄ were dispersed in 50 mL deionized water for 10 min to form a slurry using a high power ultrasonicator (JY92-IIN, China) operating at the power of 200 W. Then SnCl₂·2H₂O was added stoichiometrically after grinding in an agate mortar. Two composites were prepared with molar ratios of Sn:C of 0.3:1 and 0.8:1, respectively. (The samples were marked as L-SnO₂/CNT and H-SnO₂/CNT.) The suspensions were further dispersed by ultrasonication for 10 min, then were separated by centrifugation and dried in vacuum.

The obtained precursor was calcined at 350 ºC for 2 h. The heating rate was limited to as low as 1 ºC/min.

2032 type coin cells were assembled in an argon-filled glove box for evaluating the electrochemical properties of the composite. The electrodes were prepared by mixing 80 wt. % of the sample powder with 10 wt. % carbon black and 10 wt. % of polytetrafluoro ethylene (PTFE) binder dissolved in absolute ethanol to form a homogeneous slurry. The slurry was then spread onto nickel foam and pressed under the pressure of 10 MPa, followed by drying at 120 ºC for 12 h under vacuum. The metallic lithium sheet was used as the counter electrode. 1 M LiPF$_6$ in a 1:1:1 mixture of ethylene carbonate, dimethyl carbonate and ethylenemethyl carbonate (1 M LiPF$_6$/EC + DMC + EMC) was used as the electrolyte and Ube (25 µm) as the separator.

X-Ray diffraction (XRD) patterns were collected on a D/MAX-Ultima IV diffractometer with CuK$_\alpha$ radiation. The morphology of the as-prepared powders and dry slurry were investigated by scanning electron microscopy (LEO-1530VP, SEM). The cells were galvanostatically charged and discharged in the voltage range of 0.005-2 V at a constant current density of 200 mA g^{-1}. Cyclic voltammetry (CV) was conducted on the electrochemical working station (Gamry Instrument model PCI 4-750) at a scan rate of 0.1 mV s^{-1}.

RESULTS AND DISCUSSION

The SEM images give a general view of the SnO$_2$/CNT composite compared with bare SnO$_2$ powder. For the L-SnO$_2$/CNT, shown in Fig. 1a, only a few SnO$_2$ particles are deposited on some selected sites of CNTs, while, interestingly, the morphology of the H-SnO$_2$/CNT (Fig. 1b) reveals a three-dimensional, flower-like appearance. The higher the concentration of SnCl$_2$·2H$_2$O, the higher the amount of SnO$_2$ deposited on the surface of CNTs. Fig. 1c shows the bare SnO$_2$ particles, prepared without CNTs added, with a size of about 100 nm. The image of Fig. 1d is the SnO$_2$/CNT composite after pressed and dried in vacuum. Carbon nanotubes distribute uniformly on the surface of the layer, forming an electric network. As shown in Fig. 1e, holes and gaps can be observed clearly, in which active materials were filled. Furthermore, the coarse surface of nickel foam (Fig. 1f) consolidates the connection with active materials, resulting in better electrochemical performance.
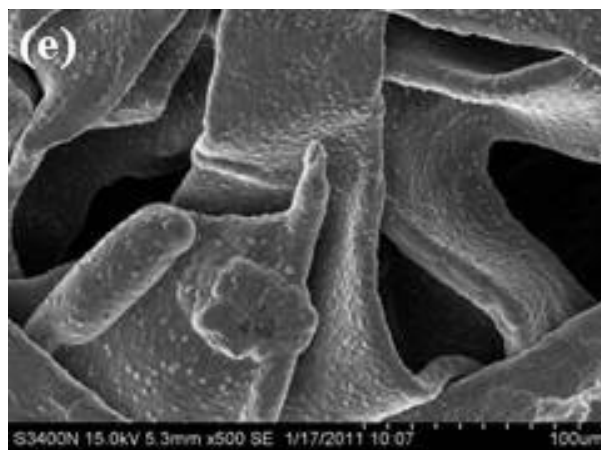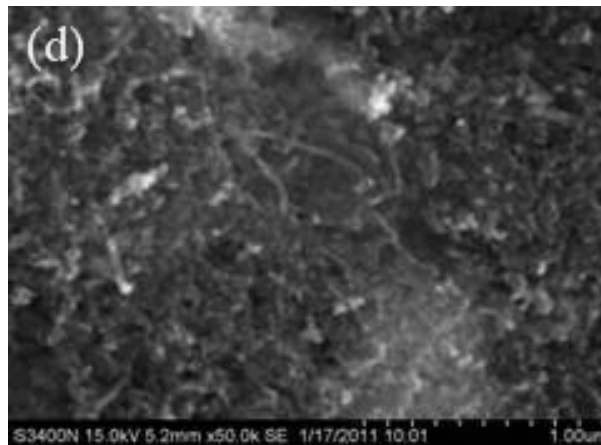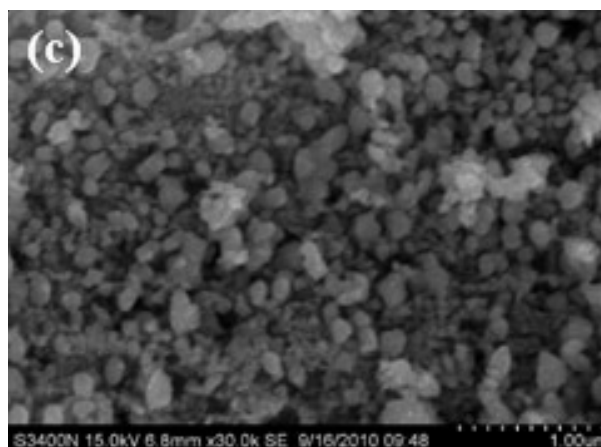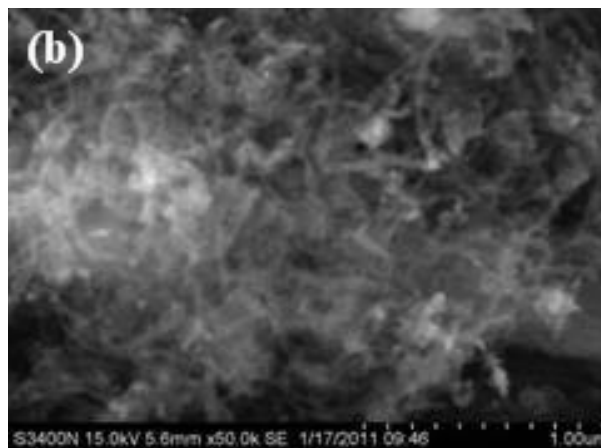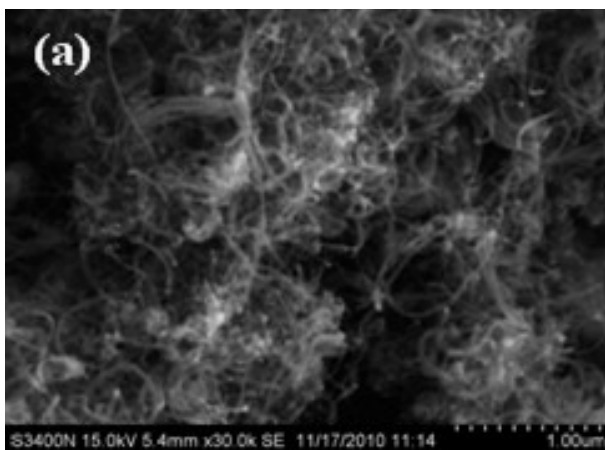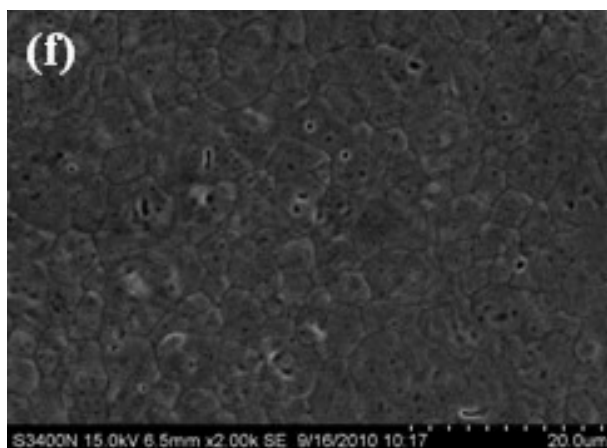
Fig. 1. SEM images of (a) L-SnO₂, (b) H-SnO₂, (c) bare SnO₂, (d) H-SnO₂ composite slurry after drying in vacuum, (e) nickel foam in low magnification and (f) nickel foam in high magnification

The structural features were confirmed by X-ray diffraction patterns (Fig. 2). The CNTs characteristic peaks are at about 26 and 43º, corresponding to the (002) and (101) reflections. For the bare SnO_2 powder, all the diffraction peaks in XRD pattern can be well indexed to powder diffraction standards (JCPDS) card (41-1445), revealing that a tetragonal rutile phase of SnO_2 was formed. For the H-SnO_2/CNT sample, peaks at 26.6, 33.8 and 51.8º, correspond to the (1 1 0), (1 0 1) and (2 1 1) reflections of SnO_2. No impurity peak was observed, indicating that high-purity SnO_2 was synthesized in the H-SnO_2/CNT composite.
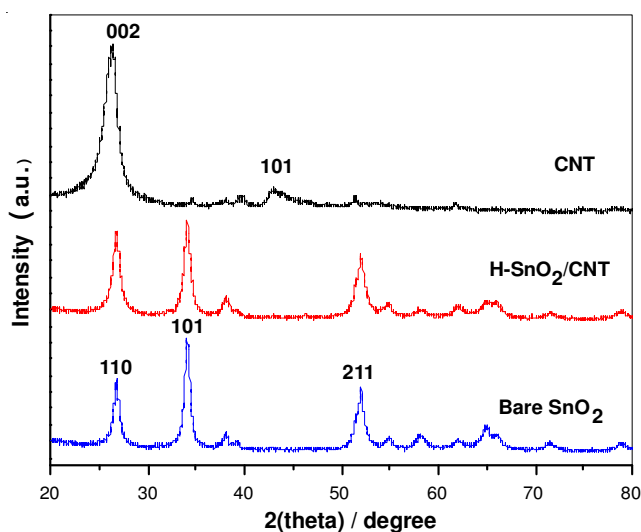
Fig. 2. X-Ray diffraction patterns of CNT, bare SnO₂ and H-SnO₂/CNT

The lithium storage capacity of the four samples was determined *via* galvanostatic charge-discharge cycling. Fig. 3 depicts the first two discharge-charge curves of samples at the current density of 200 mA g⁻¹ between 0.005 and 2 V. The composite curves of SnO_2/CNT are reported previously[19,20]. For the L-SnO_2/CNT and H-SnO_2/CNT samples, there exists a broadly defined plateau at 1.0-0.75 V which can be ascribed to the reduction of SnO_2 into Sn. In the first cycle, the irrever-sible capacity corresponding to the L-SnO_2/CNT is 1087 mAh g⁻¹, a little higher than 894 mAh g⁻¹ of the H-SnO_2/CNT compo-site. The initial coulombic efficiencies
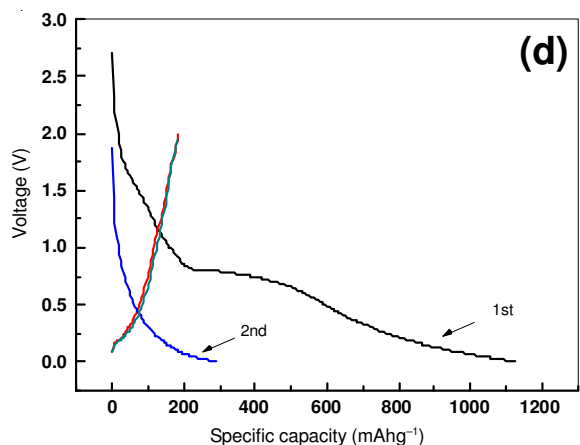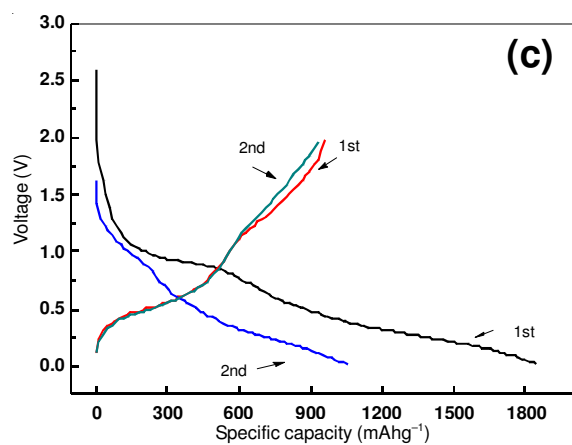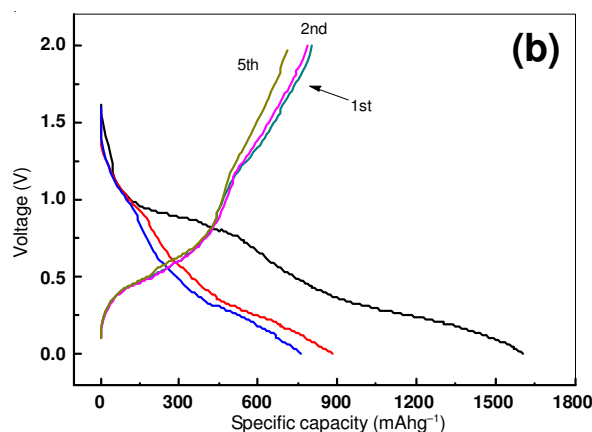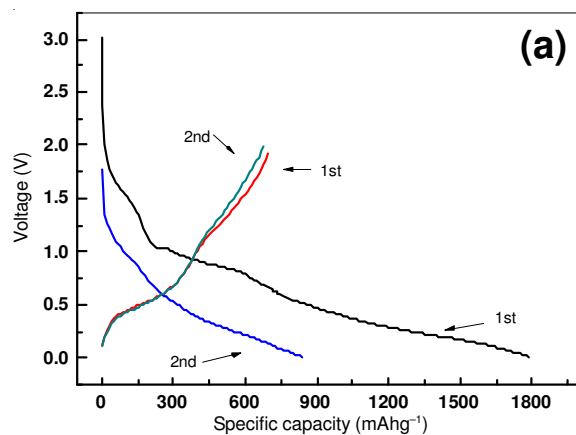
Fig. 3. Discharge-charge curves of L-SnO₂/CNT (a), H-SnO₂/ CNT (b), bare SnO₂ (c) and pure CNTs (d)

associated with the L-SnO$_2$/CNT and the H-SnO$_2$/CNT composite are 39.3 and 51.8 %, respectively. For comparison, bare SnO$_2$ and original CNTs were tested under the same electrochemical condition. The initial coulombic efficiencies of bare SnO$_2$ is almost the same with that of H-SnO$_2$/CNT composite, while the CNTs show a poor capacity retention, only 183 mAh g^{-1} in the second cycle. It is obvious that the reversible capacity of SnO$_2$/CNT composite is significantly affected by the amount of CNTs, because the nature of the solid electrolyte interface (SEI) film formed by reaction of surface groups on the CNTs with lithium determines to a large extent the irreversible capacity[21].

The results of cyclic voltammetry (CV) measurements of bare SnO$_2$ and H-SnO$_2$/CNT composite are displayed in Fig. 4. During the first scan of the bare SnO$_2$ electrode, the characteristic peak at about 0.5 V appears in the cathodic sweep process, which ascribes to the formation of SEI in eqn. 1[22], while two peaks at 0.75 and 1.3 V appear in the anodic sweep process. The current of the anodic peak at 0.75 V increases in the second cycle, corresponding to the reversible reaction in eqn. 2.

$$SnO_2 + 4Li^+ + 4e^- \rightarrow Sn + 2Li_2O \qquad (1)$$
$$Sn + xLi^+ + xe^- \leftrightarrow Li_xSn \ (0 \le x \le 4.4) \qquad (2)$$

(a)

(b)
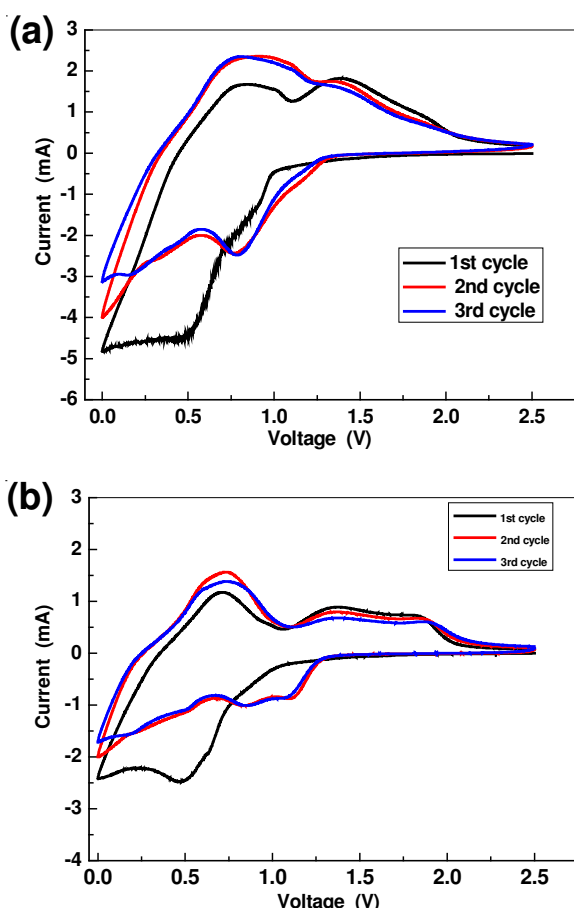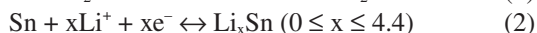
Fig. 4.   Cyclic voltammetry of bare SnO$_2$ (a) and H-SnO$_2$/CNT composite (b) at a scan rate of 0.1 mV s^{-1}

As for the H-SnO$_2$/CNT electrode, the main cathodic peak is located in the similar voltage range as that of the bare SnO$_2$. The cathodic peak is much broader and in the lower current in the second cycle. The composite sample shows reasonably

well repeated in the following cycles, revealing the good cycle stability. Interestingly, for the both samples, the peaks at 1.3 V can be clearly observed in the second and third cycles with the intensity decreased. It means the first reaction as described in eqn. 1 is reversible partially, because the Li-Sn alloying-dealloying reactions only occur below 1.0 V[23]. There are similar but not clear peaks in the curve of bare SnO$_2$.

The reversible capacity *versus* cycle number profiles of L-SnO$_2$/CNT, H-SnO$_2$/CNT, bare SnO$_2$ and pure CNT are demonstrated in Fig. 5a. Obviously, the reversible capacity of bare SnO$_2$ decreases sharply to 202 mAh/g after 30 cycles due to its large volume expansion in the process of insertion and extraction of lithium ion, while the capacity of CNTs drops slightly to *ca.* 133 mAh g^{-1}.

(a)

(b)
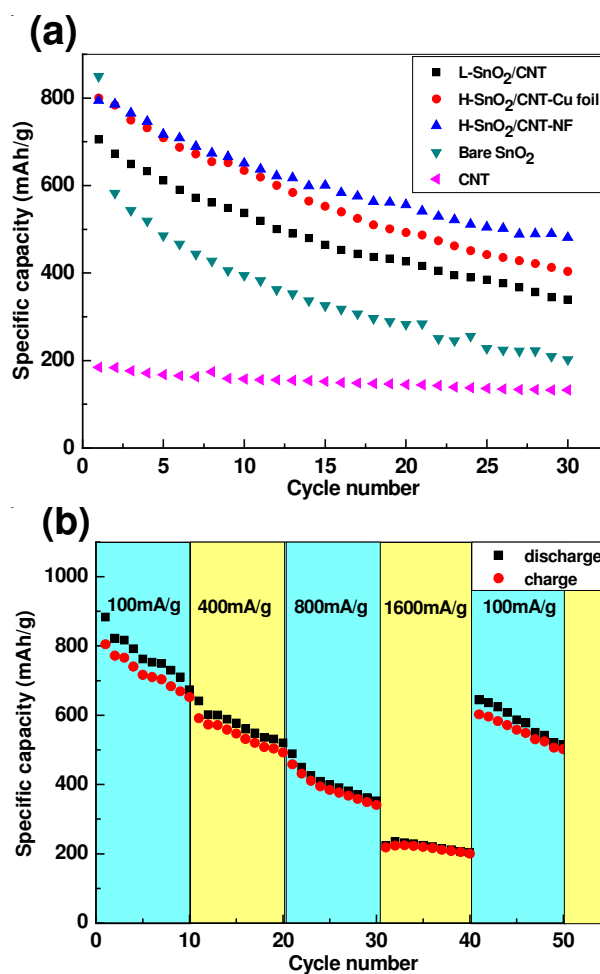
Fig. 5.   (a) Cycle performance of L-SnO$_2$/CNT, H-SnO$_2$/CNT with Cu foil, H-SnO$_2$/CNT with nickel foam, bare SnO$_2$ and pure CNTs at the current density of 200 mA g^{-1}, (b) rate capability of the H-SnO$_2$/CNT

All the SnO$_2$/CNT composites show better capacity retention, with the two H-SnO$_2$/CNT samples delivering higher capacity. The specific capacity of H-SnO$_2$/CNT sample using nickel foam still reaches as high as 481 mAh g^{-1} after 30 discharge-charge cycles. In contrast, H-SnO$_2$/CNT sample with Cu foil as a conductive collector exhibits a specific capacity of 404 mAh g^{-1} under the same condition, much lower than that using nickel foam. The main reason is that the three dimensional network and elasticity of nickel foam enhance

the connection between the composite and current collector, stabilizing the electrode structure[24]. The H-SnO$_2$/CNT with nickel foam also exhibits good rate capability, as shown in Fig. 5b. At the high current density of 1600 mA g^{-1}, it shows a good capacity (above 200 mAh g^{-1}) due to the CNTs electric conductive network (Fig. 1d). When the current density changes back to 100 mA g^{-1}, the capacity returns to 502 mAh g^{-1} after 10 cycles. Although the performance of present materials is not as good as SnO$_2$ nanowires[25], or nanorod[26], the simple and low-cost process and relatively high electrochemical performance still make them for the future commercial usage.

Conclusion

SnO$_2$/CNT composites have been prepared by a simple method of liquid-phase precipitation. The key features of this method are the simple process, low energy consumption and cheap source materials. The distribution of SnO$_2$ can be controlled by changing the molar ratio of Sn and C in the precursor. The higher SnO$_2$ content sample on nickel foam plays better electrochemical performance, because the carbon nanotubes prevent the volume expansion and the nickel foam enhances the connection with active material. In addition, it exhibits reasonable capacity when the current density is changed from a high to a small value.

REFERENCES

1. J.M. Tarascon and M. Armand, *Nature*, **414**, 359 (2001).
2. F.M. Courtel, E.A. Baranova, Y.A. Lebdeh and I.J. Davidson, *J. Power Sources*, **195**, 2355 (2010).
3. I.A. Courtney, W.R. McKinnon and J.R. Dahn, *J. Electrochem. Soc.*, **146**, 59 (1999).
4. M.N. Obrova, L. Christensen, D.B. Le and J.R. Dahn, *J. Electrochem. Soc.*, **154**, A849 (2007).
5. Y.T. Han, X. Wu, G.Z. Shen, B. Dierre, L.H. Gong, F.Y. Qu, Y. Bando, T. Sekiguchi, F. Filippo and D. Golberg, *J. Phys. Chem. C*, **114**, 8235 (2010).
6. J.S. Chen, C.M. Li, W.W. Zhou, Q.Y. Yan, L.A. Archerc and X.W. Lou, *Nanoscale*, **1**, 280 (2009).
7. L.F. Xiao, J.P. Li, Q. Li and L.Z. Zhang, *J. Solid State Electrochem.*, **14**, 931 (2010).
8. C. Wang, Y. Zhou, M.Y. Ge, X.B. Xu, Z.L. Zhang and J.Z. Jiang, *J. Am. Chem. Soc.*, **132**, 46 (2010).
9. J.P. Liu, Y.Y. Li, X.T. Huang, R.M. Ding, Y.Y. Hu, J. Jiang and L. Liao, *Chem. Mater.*, **19**, 1859 (2009).
10. X.W. Lou, J.S. Chen, P. Chen and L.A. Archer, *Chem. Mater.*, **13**, 2868 (2009).
11. X.W. Lou, C.M. Li and L.A. Archer, *Adv. Mater.*, **21**, 2536 (2009).
12. J. Yao, X.P. Shen, B. Wang, H.K. Liu and G.X. Wang, *Electrochem. Commun.*, **11**, 1849 (2009).
13. G.D. Du, C. Zhong, P. Zhang, Z.P. Guo, Z.X. Chen and H.K. Liu, *Electrochim. Acta*, **55**, 2582 (2010).
14. Y.B. Fu, R.B. Ma, Y. Shu, Z. Cao and X.H. Ma, *Mater. Lett.*, **63**, 1946 (2009).
15. Z.Y. Wang, G. Chen and D.G. Xia, *J. Power Sources*, **184**, 432 (2008).
16. C.H. Xu, J. Sun and L. Gao, *J. Phys. Chem. C*, **113**, 20509 (2009).
17. A. Dhanabalan, Y. Yu, X.F. Li, W. Chen and K. Bechtold, *J. Mater. Res.*, **25**, 1554 (2010).
18. Y. Yu, L. Gu, A. Dhanabalan, C.H. Chen and C.L. Wang, *Electrochim. Acta*, **54**, 7227 (2009).
19. Z.Y. Wang, G. Chen and D.G. Xia, *J. Power Sources*, **184**, 432 (2008).
20. S.B. Yang, H.H. Song, H.X. Yi, W.X. Liu, H.J. Zhang and X.H. Chen, *Electrochim. Acta*, **55**, 521 (2009).
21. Y.P. Wu, E. Rahm and R. Holze, *J. Power Sources*, **114**, 228 (2003).
22. J.S. Chen, Y.L. Cheah, Y.T. Chen, N. Jayaprakash, S. Madhavi, Y.H. Yang and X.W. Lou, *J. Phys. Chem. C*, **113**, 20504 (2009).
23. R.D. Cakan, Y.S. Hu, M. Antonietti, J. Maier and M.M. Titirici, *Chem. Mater.*, **20**, 1227 (2008).
24. Z. Chen, L. Christensen and J.R. Dahn, *Electrochem. Commun.*, **5**, 919 (2003).
25. P. Meduri, C. Pendyala, V. Kumar, G.U. Sumanasekera and M.K. Sunkara, *Nanolett.*, **9**, 612 (2009).
26. D.N. Lei, M. Zhang, Q.Y. Hao, L.B. Chen, Q.H. Li, E.D. Zhang and T.H. Wang, *Mater. Lett.*, **65**, 1154 (2011).